IOP Conference Series: Materials Science and Engineering

PAPER • **OPEN ACCESS**

Study on the influence of the strain rate sensitivity on the springback of the AA5086 alloy under warm forming conditions

To cite this article: D M Neto *et al* 2021 *IOP Conf. Ser.: Mater. Sci. Eng.* **1157** 012043

View the article online for updates and enhancements.

This content was downloaded from IP address 193.136.213.50 on 21/06/2021 at 12:45

Study on the influence of the strain rate sensitivity on the springback of the AA5086 alloy under warm forming conditions

D M Neto[1], M C Oliveira[1], J L Alves[2] and L F Menezes[1]

[1] CEMMPRE, Department of Mechanical Engineering, University of Coimbra, Polo II, Rua Luís Reis Santos, 3030-788 Coimbra, Portugal
[2] CMEMS, Department of Mechanical Engineering, University of Minho, Campus de Azurém, 4800-058 Guimarães, Portugal

E-mail: diogo.neto@dem.uc.pt

Abstract. Warm forming processes have been successfully applied to overcome some important drawbacks of the aluminium alloys, such as poor formability and large springback. The virtual try-out of this type of processes requires the accurate prediction of springback. The process conditions considered in this work are the ones established for the benchmark 3 – Springback of an Al-Mg alloy in warm forming conditions, proposed under the Numisheet 2016 international conference. The material under analysis is the AA5086-H111 aluminium alloy. Its mechanical behaviour is described by a Hockett-Sherby hardening law and an orthotropic yield function. The numerical analysis of the warm forming process is performed considering different yield criteria, using a strain rate-dependent flow rule. Although the material presents a positive strain rate sensitivity at 240ºC, the influence of the punch velocity on the punch force evolution is negligible due to the impact of the punch velocity on the temperature distribution in the cup. Since the hoop stress distribution on the ring (before splitting) is only slightly influenced by the punch velocity, the impact of the punch velocity on the springback is also negligible.

1. Introduction

The adoption of aluminium alloys is increasing in the automotive industry to reduce the vehicles weight and, consequently, reduce the fuel consumption and the CO_2 emission. However, these materials presents low formability [1] and high springback [2] at room temperature. Such drawbacks can be overcome using warm forming processes, i.e. by performing the deep drawing operation at an intermediate temperature, leading to a decrease of the flow stress and an increase of ductility. Furthermore, the generation of a temperature gradient from the bottom to the flange (heated die and cooled punch) improves formability [3]. Since the final stress state of the component is influenced by the temperature distribution during the forming operation, the springback effect is also reduced at warm forming conditions [2].

The warm forming conditions dictate the inclusion of the temperature and the strain rate in the modelling of the mechanical behaviour of the blank. The decrease of the flow stress with the temperature rise and the positive strain rate sensitivity for temperatures higher than 100ºC have been previously reported for the AA5086-H111 aluminium alloy [4]. On the other hand, experimental studies show that the anisotropy coefficients are rather constant from room temperature up to 200ºC. Thus, the model can assume constant values for the anisotropy parameters. Both the yield criterion and the hardening law are

Content from this work may be used under the terms of the Creative Commons Attribution 3.0 licence. Any further distribution of this work must maintain attribution to the author(s) and the title of the work, journal citation and DOI.
Published under licence by IOP Publishing Ltd

particularly important in the prediction of the final stress field in the component, which presents a direct impact on the springback. The split-ring test [5] is usually adopted to quantify the residual hoop stresses in deep drawn cups through the amount of springback.

This study aims to analyse the influence of the strain rate sensitivity on the springback of a split-ring, obtained following the non-isothermal conditions defined in Benchmark 3 of the Numisheet 2016 conference. Accordingly, the finite element simulation of the warm forming process comprises the solution of the transient heat conduction problem in addition to the rate-dependent thermo-elasto-plastic material constitutive model. The material of the blank is AA5086 aluminium alloy. The calibration of the hardening law parameters uses data from uniaxial tensile tests at different temperatures and strain rate values.

2. Warm forming process

The warm forming process and posterior split-ring opening conditions were defined in the benchmark proposed under the Numisheet 2016 conference [6]. The geometry of the forming tools used in the warm deep drawing of the cylindrical cup is schematically presented in Figure 1 (a). The punch diameter is 33 mm, while the clearance between the punch and the die is 1.125 mm, avoiding the occurrence of ironing phenomena. Both the punch and the die present a corner radius of 5 mm. The blank is circular (60 mm of diameter), obtained from a rolled sheet of AA5086-H111 aluminium alloy with 0.8 mm of nominal thickness. The deep drawing operation is performed under constant punch velocity, while the blank-holder force (5 kN) is maintained constant until the cup is fully drawn. Non-isothermal heating conditions are considered, i.e. both the die and the blank-holder are heated (240ºC), while the punch is water cooled [7].

The influence of the forming process conditions on the springback was assessed through the split-ring test, originally proposed by Demeri [5]. The springback resulting from the residual stresses is measured by the opening of a ring cut from the sidewall of the cylindrical cup [8]. In the present study, the ring (5 mm height) is cut perpendicularly to the revolution axis at 7 mm from the bottom of the cup. Since the temperature of the cylindrical cups after the warm forming operation is significantly higher than the room temperature, the cups are left to cool naturally before the cutting operation.

2.1. Finite element model

The numerical simulations were carried out with the in-house static implicit finite element code DD3IMP [9], specifically developed to simulate sheet metal forming processes. Each simulation is divided into six different stages: (i) heating of the blank within the tools; (ii) deep drawing operation; (iii) cooling of the cup; (iv) unloading the cup; (v) cutting the ring and (vi) split the ring. The heat transfer mechanisms between the heated forming tools and the blank dictate the non-isothermal conditions in this warm forming process. The thermo-mechanical problem is solved using the staggered coupled strategy proposed by Martins et al. [10].

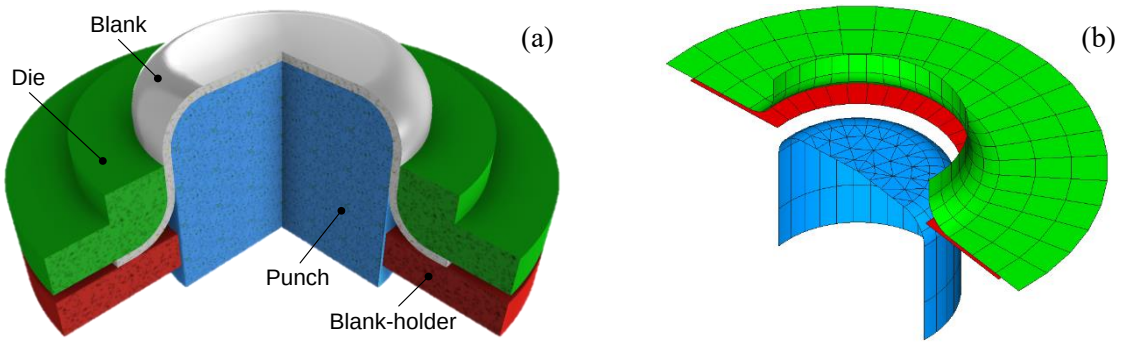

Figure 1. Warm deep drawing of a cylindrical cup: (a) scheme of the forming process; (b) discretization of the forming tools using 349 Nagata patches.

Due to geometric and material symmetry conditions, only half model is simulated, which simplifies the cutting and splitting stages. The blank is discretized using 11,970 linear hexahedral finite elements, comprising 2 layers of elements through the thickness. Although both the mechanical and the thermal problems resort to the same finite element mesh, the thermal problem uses full integration, while the mechanical problem uses the selective reduced integration technique [11]. Since forming tools are assumed rigid in the numerical model, only its outer surfaces are discretized with Nagata patches [12], as shown in Figure 1 (b). Besides, the temperature of each tool is assumed constant. Accordingly, both the die and the blank-holder are set at 240ºC, which is in agreement with the experimental observations [4]. On the other hand, although the experimental temperature of the punch increases during the forming operation, the final value is used in the numerical model, i.e. the punch is set at 70ºC.

The friction between the blank and the forming tools is modelled by the Coulomb's law, using a constant value of 0.09 for the friction coefficient value, which was estimated by Laurent et al. [7] comparing numerical and experimental punch force evolutions. The temperature of the blank is strongly dictated by the heat flow across the contacting interfaces, which is usually described by the interfacial heat transfer coefficient (IHTC). In this study, the adopted IHTC takes into account the local gap distance between the blank and the tools. Accordingly, the IHTC of the nodes in contact with the forming tools is 2500 W/m^{2}K, which decreases exponentially with the increase of the clearance according to the law presented in [13]. This allows obtaining a smooth variation of IHTC and the heat transfer coefficient in free convection (3.4 W/m^{2}K). Regarding the blank, the model also takes into account the heat generated by plastic deformation, i.e. 90% of plastic power is converted into heat. In order to assess the influence of the strain rate sensitivity on the springback, three different values of punch velocity are considered, namely 0.05 mm/s, 0.5 mm/ and 5 mm/s.

2.2. Material modelling

In the present study, the mechanical behaviour of the selected aluminium alloy is described by a rate-dependent thermo-elasto-plastic material constitutive model. The elastic behaviour is assumed isotropic and temperature-independent, which is described by the Hooke's law, using the parameters listed in Table 1. The thermal properties of the AA5086 aluminium alloy required for the finite element simulation, extracted from [4], are presented in Table 1.

Table 1. Elastic and thermal properties of the AA5086 aluminium alloy [4].

Young modulus [GPa]	Poisson's ratio	Mass density [kg/m^3]	Specific heat [J/kgºC]	Conductivity [W/mºC]
71.7	0.31	2700	900	220

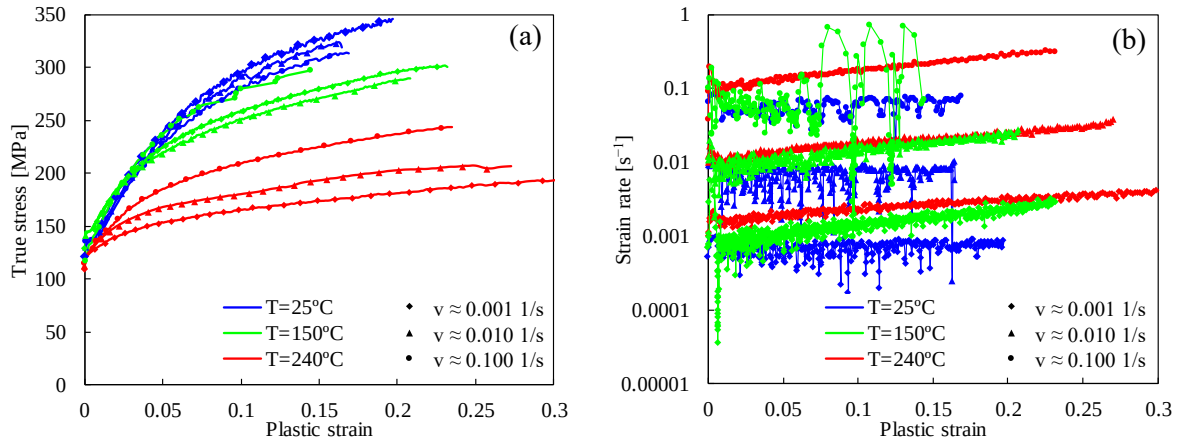

Figure 2. Experimental thermo-mechanical characterization of the AA5086 alloy: (a) stress–strain curves as a function of the temperature and strain rate; (b) evolution of the strain rate in the uniaxial tensile tests performed at different temperatures [6].

The thermo-mechanical behaviour of this aluminium alloy was assessed by the benchmark committee through uniaxial tensile tests. Figure 2 (a) presents the experimental stress–strain curves from these tests, carried out at different temperatures (25ºC, 150ºC and 240ºC) and distinct values of crosshead velocity [6]. Increasing the test temperature leads to a decrease of the flow stress and an increase of the elongation at failure. The evolution of the strain rate in each uniaxial tensile test is presented in Figure 2 (b), which increases slightly during the test, particularly for warm temperatures, due to the thermal gradient in the specimen. However, three distinct levels for the strain rate can be identified, denoted by $v \approx 0.001$ s^{-1}, $v \approx 0.01$ s^{-1} and $v \approx 0.1$ s^{-1}. The strain rate sensitivity of this aluminium alloy is more visible at warm temperatures than at room temperature, as shown in Figure 2 (a). Moreover, the flow stress decreases with the increase of the strain rate (negative strain rate sensitivity) at room temperature, while the material presents a positive strain rate sensitivity at 240ºC.

The phenomenological Hockett–Sherby hardening law [14] is used in the present study to describe the flow stress of this aluminium alloy at different values of temperature and strain rate. Thus, the isotropic work hardening is given by:

$$Y = \left\{ Y_0 + \left(Q_0 + a_1 \left(1 - \exp\left(a_2 \frac{T}{T_\mathrm{m}} \right) \right) \right) \left(1 - \exp\left(-b(\bar{\varepsilon}^\mathrm{p})^{\left\{ n_0 - n_1 \left(\frac{T}{T_\mathrm{m}} \right) \right\}} \right) \right) \right\} \left(\frac{\dot{\varepsilon}}{\dot{\varepsilon}_0} \right)^{\left\{ m_0 \exp\left(m_1 \frac{T}{T_\mathrm{m}} \right) \right\}}, \quad (1)$$

where $\bar{\varepsilon}^\mathrm{p}$ represents the equivalent plastic strain, $\dot{\varepsilon}$ is the strain rate and T is the temperature. The material parameters are Y_0, Q_0, a_1, a_2, b, n_0, n_1, m_0, m_1 and $\dot{\varepsilon}_0$, while T_m denotes the melting temperature.

The parameters of the Hockett–Sherby hardening law were obtained through the minimization of the difference between the numerical and the experimental stress values. The optimization problem consists in identifying the set of material parameters $\boldsymbol{\vartheta}$ that minimizes the following error function:

$$F(\boldsymbol{\vartheta}) = \sum_{i=1}^{3} \sum_{j=1}^{3} \left\{ \sum_{k=1}^{n_{ij}} \left(\sigma_{\mathrm{exp}}^{ij}(k) - \sigma_{\mathrm{num}}^{ij}(k) \right)^2 \right\}, \quad (2)$$

where the first two sums represent the nine uniaxial tensile tests carried out at different isothermal conditions, such that (i = 25ºC, 150ºC and 240ºC) and different strain rate values (j = 0.001 s^{-1}, 0.01 s^{-1} and 0.1 s^{-1}). The total number of measured points in each uniaxial tensile test is denoted by n_{ij}. The subscripts "exp" and "num" denote the experimental and numerical data, respectively. The obtained material parameters for the isotropic hardening law are listed in Table 2. Both the melting temperature T_m and the constant strain rate normalisation factor $\dot{\varepsilon}_0$ (minimum value of strain rate available in the experimental data) were assumed as fixed in the optimization procedure.

Table 2. Material parameters of the Hockett–Sherby hardening law: AA5086 aluminium alloy.

Y_0 [MPa]	Q_0 [MPa]	a_1 [MPa]	a_2	b	n_0	n_1	m_0	m_1	$\dot{\varepsilon}_0$ [s^{-1}]	T_m[ºC]
107.07	286.81	17.43	6.32	5.92	0.78	0.32	4.2×10^{-4}	11.58	0.001	600

The Hockett–Sherby hardening law, with the parameters listed in Table 2, leads to the numerical stress–strain curves presented in Figure 3 (a), comparing different values of temperature (25ºC, 150ºC and 240ºC) and strain rate (0.001 s^{-1}, 0.01 s^{-1} and 0.1 s^{-1}). Since the variation of the initial yield stress with the temperature is negligible in this aluminium alloy (see Figure 2 (a)), the initial yield stress predicted by this constitutive model is temperature-independent at the lower strain rate value, as highlighted in Figure 3 (a). Moreover, the model predicts a positive strain rate sensitivity at warm temperatures, vanishing at room temperature. The prediction of a large positive strain rate sensitivity at 240ºC is in good agreement with the experimental observations (compare Figure 2 (a) and Figure 3 (a)). Thus, considering the non-isothermal warm forming at 240ºC, the thermo-mechanical behaviour of this aluminium alloy seems to be accurately described by this hardening law.

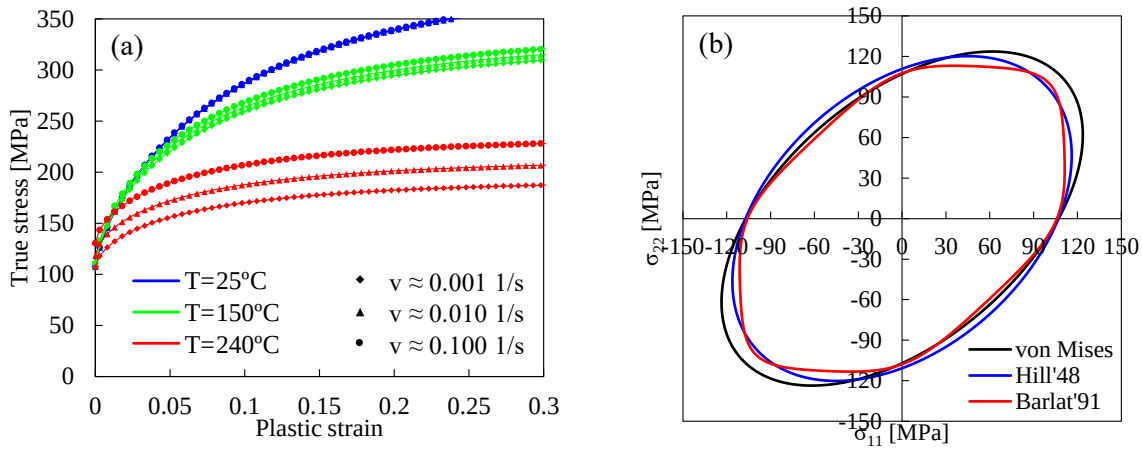

Figure 3. Mechanical modelling of the AA5086 alloy: (a) stress–strain curves for three different values of temperature and strain rate; (b) comparison of different yield surfaces.

The plastic anisotropy of this aluminium alloy was modelled using two different yield criteria, namely the Hill'48 yield criterion and the non-quadratic Barlat'91 yield criterion [15], both assumed temperature-independent in the present study. The parameters of the Hill'48 yield criterion were evaluated based on the anisotropy coefficients (*r*-values) measured at 240ºC. The sheet is assumed isotropic through the thickness direction, leading to $L=M=1.5$. Besides, since the material parameters of the hardening law (see Table 2) were obtained using the stress–strain curves in the rolling direction, the condition $G+H=1$ is imposed, leading the parameters listed in Table 3. The parameters of the Barlat'91 yield criterion were evaluated using both the yield stresses and the anisotropy coefficients, measured at 240ºC. The parameters defining the anisotropic behaviour through the thickness direction are assumed isotropic, i.e. $c_4=c_5=1.0$. The adopted procedure, currently implemented in DD3MAT in-house code [16], is based on the minimization of an error function that evaluates the difference between the predicted and the experimental values, for the yield stresses and the anisotropy coefficients. The obtained material parameters are listed in Table 3. The yield surface predicted by each yield criterion is shown in Figure 3 (b) for the $\sigma_{11}-\sigma_{22}$ plane. The anisotropic yield criteria provide distinct shapes for the yield surface, both globally inside the von Mises yield locus in the biaxial stress path.

Table 3. Material parameters for Hill'48 and Barlat'91 yield criteria.

Hill'48	*F*	*G*	*H*	*L*	*M*	*N*
	0.5597	0.6250	0.3750	1.5000	1.5000	1.6349
Barlat'91	c_1	c_2	c_3	c_4	c_5	c_6
	1.0502	1.0830	0.9355	1.0000	1.0000	1.0406

3. Results and discussion

Heating the die and the blank-holder (240ºC) while cooling the punch (70ºC) generates a temperature gradient from the bottom to the flange of the cup. The predicted temperature distribution in the cylindrical cup is presented in Figure 4 (a), for a punch displacement of 15 mm (considering 5 mm/s of punch velocity and the Hill'48 yield criterion). The temperature distribution is roughly axisymmetric, presenting its minimum in the bottom centre (P2) and the maximum in the flange. The region of the cup in contact with the punch (at 70ºC) presents the lower temperature, while the temperature of the flange is approximately the temperature of the die/blank-holder (240ºC), as shown in Figure 4 (a). The influence of the punch velocity on the predicted temperature distribution is presented in Figure 4 (b), comparing the temperature evolution of two different points (P1 and P2 identified in Figure 4 (a)). The decrease of the punch velocity yields a global decrease of the cup temperature due to the increase of the time to promote heat loses with the cold punch, as highlighted in Figure 4 (b).

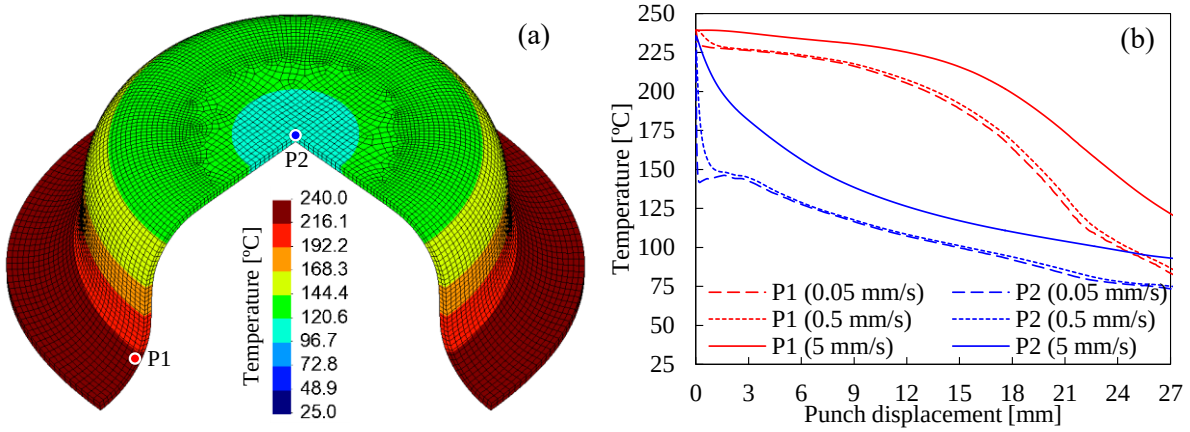

Figure 4. Predicted temperature in the cylindrical cup using the Hill'48 yield criterion: (a) temperature distribution for 15 mm of punch displacement and 5 mm/s of punch velocity; (b) evolution of the temperature in two different points (P1 and P2) for different values of punch velocity.

The predicted punch force evolution is presented in Figure 5 (a), comparing different values of punch velocity. The predicted punch force is influenced by the temperature distribution and the strain rate in the cup. The evolution of the plastic strain rate, evaluated in a point initially located in the flange (5 mm from the perimeter), is shown in Figure 5 (b) for three different values of punch velocity. Considering 5 mm/s of punch velocity, the plastic strain rate ranges from about 0.01 s^{-1} up to 0.1 s^{-1}. Besides, the relationship between the punch velocity and the predicted plastic strain rate is approximately linear, i.e. the decrease of the punch velocity leads to a decrease of the plastic strain rate in the same order. Since the strain rate arising in the experimental uniaxial tensile tests (see Figure 2 (b)) is identical to the one predicted for the warming forming (see Figure 5 (b)), the adopted range for punch velocity values is in agreement with the crosshead velocity values used in the uniaxial tensile tests.

The impact of the punch velocity on the punch force is less significant than the strain rate sensitivity of the material at 240ºC, as highlighted by the comparison Figure 3 (a) and Figure 5 (a). This is a consequence of the temperature of the cup, which is lower than 240ºC in the flange (see Figure 4 (b) and also dependent from the adopted punch velocity. The punch force evolution presents an increase when the punch velocity increases from 0.05 mm/s to 0.5 mm/s due to the positive strain rate sensitivity, while the cup temperature is approximately the same. On the other hand, the increase of the punch velocity to 5 mm/s leads to a slight decrease of the punch force due to the increase of the global temperature (see Figure 4 (b)), which cancels the positive effect of the strain rate sensitivity.

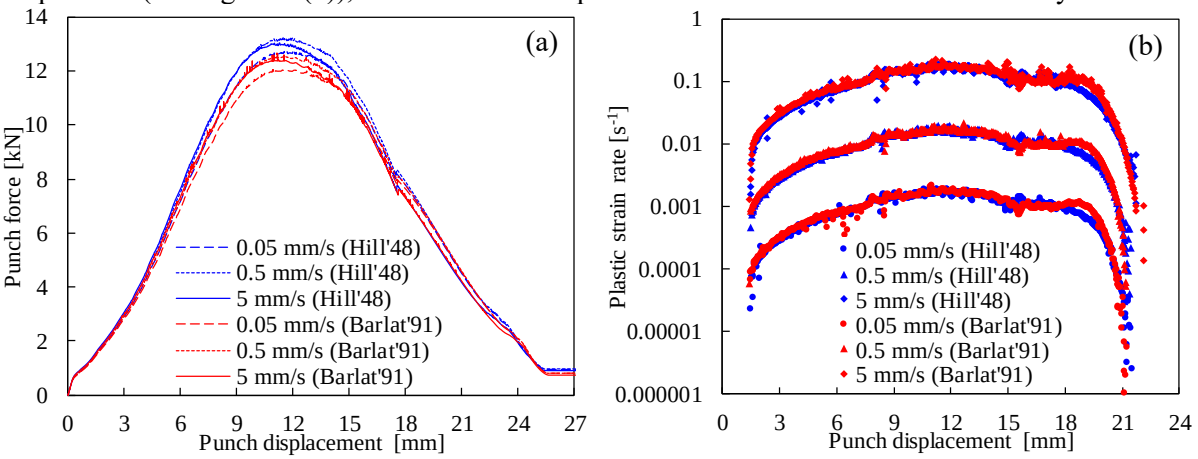

Figure 5. Influence of the punch velocity on the numerical prediction using two yield functions: (a) punch force evolution; (b) evolution of the plastic strain rate in the point P1.

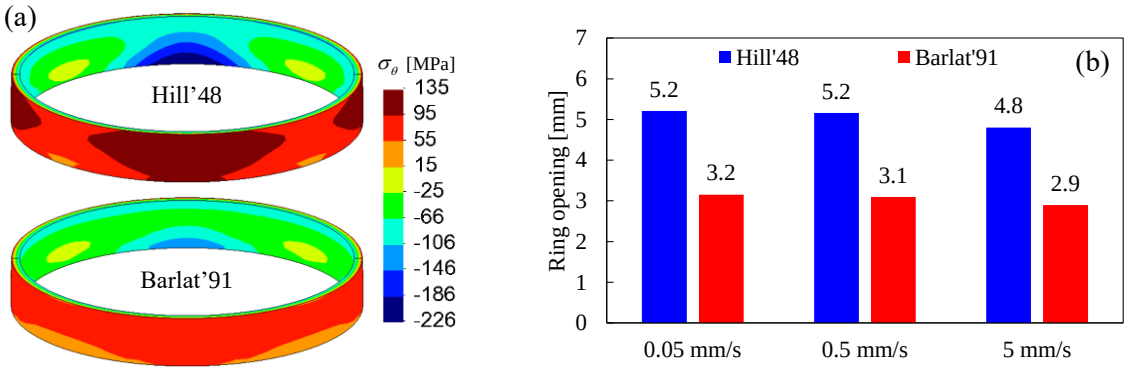

Figure 6. Influence of the punch velocity on the predicted springback using two yield criteria: (a) numerical distribution of the hoop stress on the ring before splitting using 5 mm/s of punch velocity; (b) predicted values of ring opening.

The numerical analysis of the split-ring test (after cooling down to room temperature) was carried out with the in-house code DD3TRIM, comprising the geometrical trimming and the remapping of the state variables [17,18]. The predicted distribution of the hoop stress on the ring (before splitting) is presented in Figure 6 (a) for 0.05 mm/s of punch velocity. The predicted hoop stress is compressive in the inner surface of the ring and tensile on the outer surface, presenting a slight variation along the circumferential direction due to the plastic anisotropy. The predicted values of ring opening are presented in Figure 6 (b) for the three different values of punch velocity, which result from the integration of the hoop stress over the ring thickness [19]. The impact of the punch velocity on the springback value is negligible. This results from the fact that the springback (split of the ring) is always evaluated at room temperature and the final strain distribution of the cylindrical cup is not significantly influenced by the punch velocity. On the other hand, the low value of the ring opening predicted by the Barlat'91 yield criterion (see Figure 6 (b)) is motived by the lower hoop stress gradient through the thickness integrated over the circumferential direction (see Figure 6 (a)).

4. Conclusions

This study presents the warm forming simulation of a cylindrical cup (heated die/blank-holder and cooled punch). The effect of the strain rate sensitivity (controlled by the punch velocity) on the springback is evaluated by means of the split-ring test. The numerical analysis is carried out using a rate-dependent thermo-elasto-plastic material constitutive model. The mechanical behaviour of the AA5086 alloy is described by the Hockett–Sherby hardening law, using experimental data from uniaxial tensile tests performed at different temperatures (25ºC, 150ºC and 240ºC) and distinct values of strain rate (0.001 s^{-1}, 0.01 s^{-1} and 0.1 s^{-1}) to calibrate the material parameters. The adopted yield functions (Hill'48 and Barlat'91) are assumed temperature-independent and the material parameters are calibrated using data at 240ºC. The predicted punch force evolution is dictated both by the temperature and the strain rate in the cup. However, it is not significantly influenced by the punch velocity because the positive strain rate sensitivity of the material at warm temperatures is cancelled by the decrease of the flow stress, due to the higher temperature for fast punch velocity (less cooling time). The impact of the punch velocity on the springback is negligible. Indeed, the hoop stress distribution on the ring (before splitting) is only slightly influenced by the punch velocity. However, the predicted springback is strongly influenced by the yield function adopted to model the material anisotropy. Finally, it should be mentioned that it is expected that the ring opening prediction can be improved taking into account both the Young modulus degradation and its decrease with the increase of temperature.

Acknowledgments

The authors would like to acknowledge the funding from of the Foundation for Science and Technology (FCT) under projects with reference PTDC/EME-EME/30592/2017 and PTDC/EME-EME/31657/2017

and by European Regional Development Fund through the Portugal 2020 program and the Centro 2020 Regional Operational Programme under the project MATIS and UIDB/00285/2020.

References

[1] Kim H S, Koç M, Ni J and Ghosh A 2006 Finite Element Modeling and Analysis of Warm Forming of Aluminum Alloys—Validation Through Comparisons With Experiments and Determination of a Failure Criterion *J. Manuf. Sci. Eng.* **128** 613
[2] Grèze R, Manach P Y, Laurent H, Thuillier S and Menezes L F 2010 Influence of the temperature on residual stresses and springback effect in an aluminium alloy *Int. J. Mech. Sci.* **52** 1094–100
[3] Palumbo G, Sorgente D, Tricarico L, Zhang S H and Zheng W T 2007 Numerical and experimental investigations on the effect of the heating strategy and the punch speed on the warm deep drawing of magnesium alloy AZ31 *J. Mater. Process. Technol.* **191** 342–6
[4] Neto D M, Martins J M P, Cunha P M, Alves J L, Oliveira M C, Laurent H and Menezes L F 2018 Thermo-mechanical finite element analysis of the AA5086 alloy under warm forming conditions *Int. J. Solids Struct.* **151** 99–117
[5] Demeri M Y, Lou M and Saran M J 2000 A Benchmark Test for Springback Simulation in Sheet Metal Forming
[6] Manach P Y, Coër J, Jégat A, Laurent H and Yoon J W 2016 Benchmark 3 - Springback of an Al-Mg alloy in warm forming conditions *J. Phys. Conf. Ser.* **734** 022003
[7] Laurent H, Coër J, Manach P Y, Oliveira M C and Menezes L F 2015 Experimental and numerical studies on the warm deep drawing of an Al–Mg alloy *Int. J. Mech. Sci.* **93** 59–72
[8] Laurent H, Grèze R, Manach P Y and Thuillier S 2009 Influence of constitutive model in springback prediction using the split-ring test *Int. J. Mech. Sci.* **51** 233–45
[9] Menezes L F and Teodosiu C 2000 Three-dimensional numerical simulation of the deep-drawing process using solid finite elements *J. Mater. Process. Technol.* **97** 100–6
[10] Martins J M P, Neto D M, Alves J L, Oliveira M C, Laurent H, Andrade-Campos A and Menezes L F 2017 A new staggered algorithm for thermomechanical coupled problems *Int. J. Solids Struct.* **122**–**123** 42–58
[11] Hughes T J R and Winget J 1980 Finite rotation effects in numerical integration of rate constitutive equations arising in large-deformation analysis *Int. J. Numer. Methods Eng.* **15** 1862–7
[12] Neto D M, Oliveira M C, Menezes L F and Alves J L 2014 Applying Nagata patches to smooth discretized surfaces used in 3D frictional contact problems *Comput. Methods Appl. Mech. Eng.* **271** 296–320
[13] Neto D M, Pais M, Oliveira M C, Alves J L and Menezes L F 2019 Thermomechanical analysis of the draw bead test *Adv. Mater. Process. Technol.* **5** 401–17
[14] Hockett J E and Sherby O D 1975 Large strain deformation of polycrystalline metals at low homologous temperatures *J. Mech. Phys. Solids* **23** 87–98
[15] Barlat F, Lege D J and Brem J C 1991 A six-component yield function for anisotropic materials *Int. J. Plast.* **7** 693–712
[16] Barros P D, Carvalho P D, Alves J L, Oliveira M C and Menezes L F 2016 DD3MAT - a code for yield criteria anisotropy parameters identification. *J. Phys. Conf. Ser.* **734** 032053
[17] Baptista A J, Alves J L, Rodrigues D M and Menezes L F 2006 Trimming of 3D solid finite element meshes using parametric surfaces: Application to sheet metal forming *Finite Elem. Anal. Des.* **42** 1053–60
[18] Miguel C, Neto D M, Oliveira M C, Alves J L and Menezes L F 2018 Incremental volumetric and Dual Kriging remapping methods *Finite Elem. Anal. Des.* **139** 35–48
[19] Simões V M, Oliveira M C, Neto D M, Cunha P M, Laurent H, Alves J L and Menezes L F 2018 Numerical study of springback using the split-ring test: influence of the clearance between the die and the punch *Int. J. Mater. Form.* **11** 325–37